


Article

# Urban Heat Island Analysis over the Land Use Zoning Plan of Bangkok by Means of Landsat 8 Imagery

Chaiyapon Keeratikasikorn <sup>1</sup> and Stefania Bonafoni <sup>2,\*</sup> 

<sup>1</sup> Department of Computer Science, Khon Kaen University, Khon Kaen 40002, Thailand; chaiyapon@kku.ac.th

<sup>2</sup> Department of Engineering, University of Perugia, via Duranti 93, 06125 Perugia, Italy

\* Correspondence: stefania.bonafoni@unipg.it; Tel.: +39-075-585-3663

Received: 2 February 2018; Accepted: 9 March 2018; Published: 11 March 2018

**Abstract:** Surface urban heat island (SUHI) maps retrieved from spaceborne sensor data are increasingly recognized as an efficient scientific support to be considered in sustainable urban planning. By means of reflective and thermal data from Landsat 8 imagery in the time interval 2014–2016, this work deals with the SUHI pattern identification within the different land use categories of Bangkok city plan. This study first provides an overview of the SUHI phenomenon in Bangkok, then singles out the surface heating behavior in each land use category. To describe the SUHI dynamics within the different classes, the main statistics of the SUHI intensity (mean, standard deviation, maximum and minimum) are computed. Overall, the analysis points out that the categories placed in the city core (high-density residential; commercial; historical and military classes) exhibit the highest mean SUHI intensities (around 4 °C); whilst the vegetated pixels exert a less cool effect with respect to the greenery of categories mainly placed farther from the city center. The proposed analysis can help to identify if the land use plan requires targeted future actions for the SUHI mitigation; or if the maintenance of the current urban development model is in line with the environmental sustainability.

**Keywords:** surface urban heat island; Bangkok; Landsat 8; urban planning; SUHI pattern

## 1. Introduction

The urbanization process, responsible for several environmental effects, is increasingly addressed with the analysis of the well-known urban heat island (UHI) phenomenon. The UHI can be described as an anthropogenic warming modification of the urban environment having involvements in human comfort and health, air pollution, urban planning and development policy, energy management [1–4]. The urban land changes, particularly when vegetated areas are replaced by impervious surfaces, cause the increase of the sensible heat flux, the trapping and absorption of solar irradiation on urban surfaces and the resulting canyon phenomenon [5–7]. Consequently, air and surface temperatures exhibit a difference between urban area and rural surroundings [8,9], quantified in terms of UHI intensity.

Several studies assessed the UHI intensity by using in situ weather stations measuring air temperature in rural and urban sites: however, the stations, unevenly distributed, do not permit a global view over the study area. Some experimental campaigns can combine airborne hyperspectral observations and in situ measurements [10], but aircrafts have restricted or sporadic overpass times.

Usually air temperature exhibits a nighttime UHI that is less detectable during daytime [11,12]. Instead, surface temperatures give rise to a surface urban heat island (SUHI) exhibiting its effects throughout the diurnal cycle, with a maximum intensity in the daytime [12,13].

Typically, the SUHI is obtained from remote sensing data provided by spaceborne sensors, exploiting their spatial coverage and revisit time [9,14]. Advances in satellite mission features and in data availability have fostered a great number of SUHI studies in different urban areas around the world providing spatial and temporal analysis of the urban heating patterns.

Among the potential applications, the SUHI maps derived from spaceborne sensors supply a scientific support for the urban planning policy aimed to integrate urban development and landscape ecosystems [15,16]. For instance, the widespread presence of impervious surfaces is a significant urbanization factor increasing the SUHI effects [17], whilst vegetation and green spaces in the urban texture are one of the fundamental strategies to decrease the urban warming intensity [18,19]. A review of the potential strategies to mitigate the SUHI effects and applicable in the design phase of urban development is found in [20].

The above considerations suggest how the SUHI pattern is influenced by external factors, e.g., city location and atmospheric conditions, and intrinsic factors, e.g., city size and growth, human activities and traffic, land use within the urban area [21]. The use of remote sensing data to study the SUHI spatial and temporal trend can be of practical utility in providing indications to plan and regulate the intrinsic factors [22].

However, the land use heterogeneity of surfaces within an urban texture (e.g., low/high density residential zone, commercial or industrial zone, military or historical zone, government or public area, etc.) has very often been neglected in the SUHI analysis. Such heterogeneity is clearly detailed by the land use zoning plan provided by the municipal government in the context of the urban development policy. The indications of the SUHI intensity within each sub-category, with well-defined borders, are essential to assess the urban policy effectiveness in terms of sustainability.

By means of satellite imagery, this work addresses the issue of the SUHI pattern identification within the different land use categories reported in the city plan of Bangkok, to evaluate the potential surface heating variability. First, land surface temperature (LST) maps were retrieved by using Landsat 8 images acquired in the time interval 2014–2016, with a pixel size resampled at 30 m from the native 100 m spatial resolution of the thermal bands. Then, the correspondent SUHI maps were derived and compared with the last Bangkok comprehensive land use plan, in order to single out the specific heating pattern in the different urban zones. This analysis not only describes the current situation, but also provides a perspective insight of the municipal land use plan policy.

Usually, satellite SUHI maps are compared with the Land Use and Land Cover (LULC) maps retrieved from Landsat reflective images: the government land use plan categories, also outlined in perspective, are different from the satellite LULC ones in terms of number, type, size, pixel composition and boundaries.

From literature, the urban heat island studies in Bangkok are limited: UHI intensity investigations were carried out with in situ weather stations measuring air temperature [23–25], while satellite maps from MODerate-resolution Imaging Spectroradiometer (MODIS), with a spatial resolution of 1 km, were processed from September 2001 to March 2002 to quantify the SUHI [26]. Therefore, this study also represents a SUHI insight of the megacity at higher spatial resolution.

## 2. Study Area

The study area is Bangkok, the capital of Thailand (city center coordinates: latitude 13.83°N, longitude 100.54°E): location and urban extension are reported in Figure 1.

Bangkok, the most populous and largest city in Thailand, occupies about 16,000 km<sup>2</sup> with a population of 8.2 million (6.3 million within the municipality). It is seated in the Chao Phraya River delta in the Thailand central plain; the river course through Bangkok ends into the Gulf of Thailand 25 km south of the city center. The urban area is flat (mean elevation of 1.5 m above sea level) and the closest mountain is located 40 km southeast of the city. A serious problem for Bangkok is the subsidence, since the city is subject to flood risk due to its low-lying topography and insufficient drainage infrastructures.

There are several parks in Bangkok, even though the overall green space for the whole city is moderate, especially in the denser built-up zones (1.8 m<sup>2</sup> per person), at least 10 times less than in other cities across Asia [27].

It has a tropical wet and dry climate, influenced by the South Asian monsoons. Even though air temperatures are almost warm during the year, ranging from a mean value of 22 °C in December to 35 °C in April, in the Central Thailand three seasons are experienced: Winter, summer and rainy season. The winter season approximately takes place between November and mid-February, when the summer season begins until mid-May. The rainy season starts around mid-May until October. The dry northeast monsoon occurs between October and February, when the summer season starts. The lowest recorded air temperature was 10 °C in January 1955, the highest 40 °C in April 1979 [28].

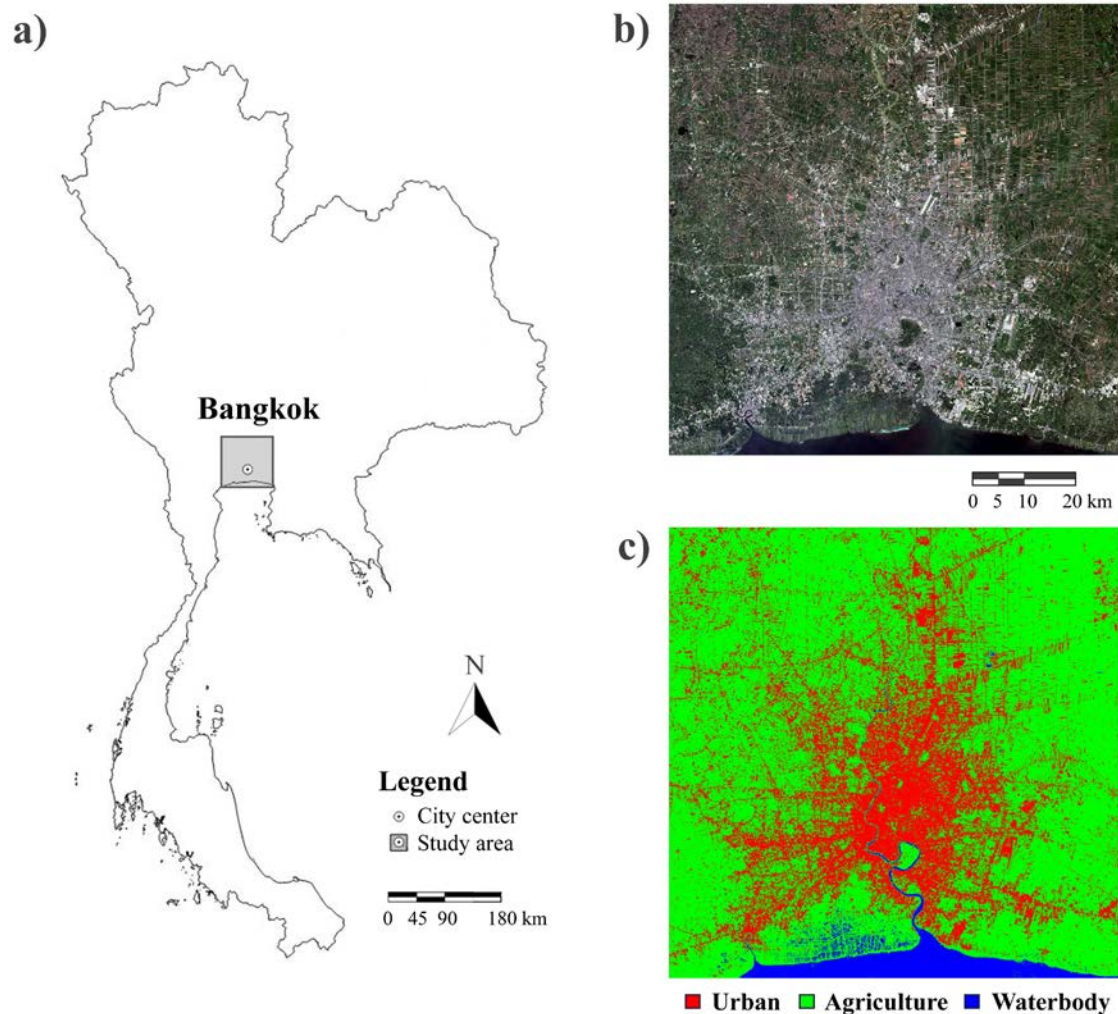


**Figure 1.** (a) Bangkok (city center coordinates: latitude 13.83°N, longitude 100.54°E) inside the Thailand administrative borders. (b) Bangkok area from Landsat 8 RGB image of 17 November 2014. (c) Land Use and Land Cover (LULC) map of Bangkok obtained from Landsat 8 data (see Section 3.2).

Bangkok presents an administrative subdivision in 50 districts: 35 districts are located east of the Chao Phraya River, 15 in the west part. The Bangkok Metropolitan Administration (BMA), i.e., the government of the city, has organized these districts into groups for management policies and urban planning aims, the latter including the land use plan under the responsibility of the City Planning Department. Figure 2 shows the last comprehensive land use zoning plan (effective from 2013) regulating the 50 districts [29], whilst Figure 3 represents the zoning plan boundary, i.e., the 50 district external boundary, superimposed on the Bangkok area of Figure 1b.

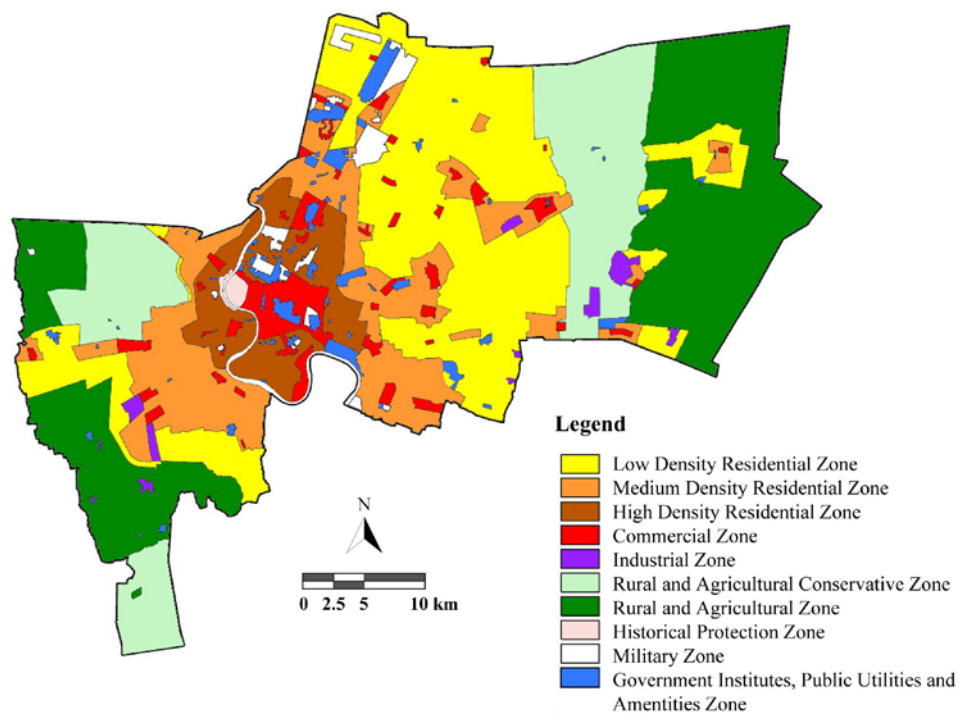


**Figure 2.** The last comprehensive land use zoning plan of Bangkok (effective from 2013) within the 50 district boundary [29].

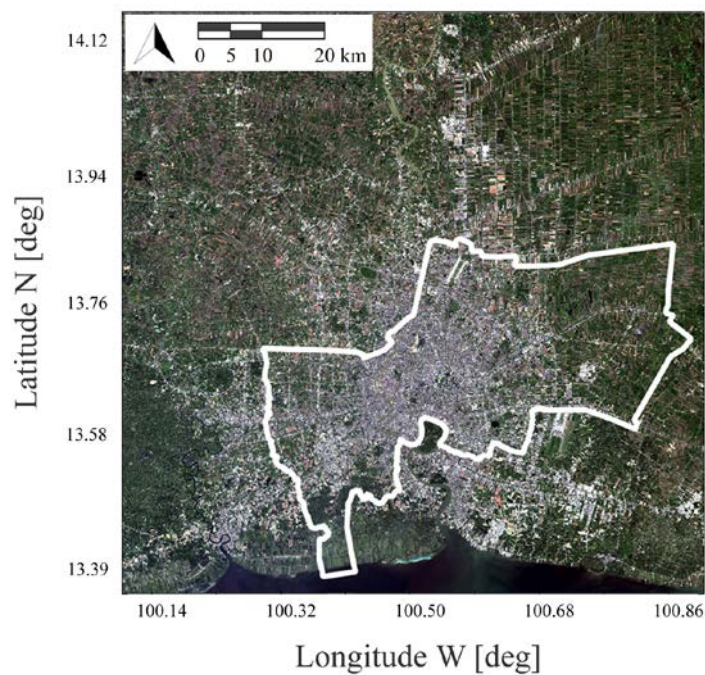


**Figure 3.** Zoning plan external boundary superimposed on the Bangkok area obtained by Landsat 8 RGB image of 17 November 2014.

With reference to Figure 2, the ten land use categories of the plan are: Low/Medium/High-density Residential zones, Commercial and Industrial zones, Agricultural and Rural Conservation zones, Historical Protection zone, Military zone, Public Utilities zone.

### 3. Data Sets and Methods

#### 3.1. Landsat 8 Data

The Landsat 8 satellite carries two sensors, the Operational Land Imager (OLI) and the Thermal Infrared Sensor (TIRS). The OLI sensor has seven reflective bands in the visible, near infrared and short-wavelength infrared, plus two further panchromatic and cirrus bands. TIRS has two bands in the thermal infrared (TIR) region. OLI channels have a spatial resolution of 30 m, TIRS channels of 100 m. TIRS bands are delivered at 30 m, after resampling with cubic convolution, by the US Geological Survey (USGS) [30]. In this study, surface reflectances and TIR radiances provided by USGS were used.

Concerning the LST estimation from TIRS observations, Yu et al. [31] showed that LST retrieved by the radiative transfer equation (RTE) method using TIRS Band 10 (10.60  $\mu\text{m}$ –11.19  $\mu\text{m}$ ) has the highest accuracy with respect to other methods, and LST estimated from TIRS Band 10 has better accuracy than TIRS Band 11 (11.50  $\mu\text{m}$ –12.51  $\mu\text{m}$ ).

Therefore, LST from TIRS\_B10 data was obtained by inverting the RTE according to:

$$L_{sens,\lambda} = \left[ \varepsilon_{\lambda} B_{\lambda}(T_s) + (1 - \varepsilon_{\lambda}) L_{\lambda}^{\downarrow} \right] \tau_{\lambda} + L_{\lambda}^{\uparrow} \quad (1)$$

where:

- $L_{sens,\lambda}$ : At-sensor radiance at the top-of-atmosphere;
- $\varepsilon_{\lambda}$ : Surface emissivity;
- $B_{\lambda}(T_s)$ : Planck's law where  $T_s$  is the LST;
- $L_{\lambda}^{\downarrow}$ : Downwelling atmospheric radiance;
- $\tau_{\lambda}$ : Total atmospheric transmissivity of the atmosphere;
- $L_{\lambda}^{\uparrow}$ : Upwelling atmospheric radiance.

LST is retrieved from (1) by inversion of the Planck's law [32], known the surface emissivity. The atmospheric parameters  $\tau_{\lambda}$ ,  $L_{\lambda}^{\downarrow}$  and  $L_{\lambda}^{\uparrow}$  were estimated by means of a web-based tool [33] that uses the National Centers for Environmental Prediction (NCEP) atmospheric profiles as inputs to the MODTRAN radiative transfer software [34]. Land surface emissivity was computed by the Normalized Difference Vegetation Index (NDVI) threshold method as in [35,36]. Although the NDVI is a common approach for emissivity estimation from Landsat images, it can be inaccurate over particular manmade surfaces, as proved in [37].

The Landsat 8 passages in clear-sky conditions over Bangkok, in the mission operative period 2013–2017, are reported in Table 1; passages are at around 10:40 local time, where local time is +7:00 from UTC time. Landsat 8 covers the same area on the Earth every 16 days.

**Table 1.** Landsat 8 passages in clear-sky conditions over Bangkok.

Date	Path	Row
2 February 2014	129	50, 51
17 November 2014	129	50, 51
4 January 2015	129	50, 51
20 January 2015	129	50, 51
5 February 2015	129	50, 51
6 December 2015	129	50, 51
12 April 2016	129	50, 51

### 3.2. SUHI Computation

The warming effect in an urban area can be quantified by the SUHI intensity, computed as the surface temperature difference between urban ( $LST_{urban}$ ) and rural ( $LST_{rural}$ ) pixels:

$$SUHI = LST_{urban} - LST_{rural} \quad (2)$$

$LST_{rural}$  can be considered as a reference or a bias value and, in this work, was computed as the LST average over the rural pixels in a buffer area of few kilometers surrounding the Bangkok urban area. Water pixels were discarded from the rural buffer. SUHI intensity is not an absolute temperature, but a temperature difference that, consequently, tend to weaken local weather condition effects and other error sources [26].

For the Equation (2) evaluation, the identification of built-up and rural pixels is performed by the Land Use and Land Cover (LULC) map derived from the Landsat OLI images (Figure 1c). The land covers were classified into three types (built-up, cropland, water body) applying a supervised maximum likelihood classification approach [38,39]. The classified map reliability was assessed by using the high-resolution images in GoogleEarth Pro<sup>®</sup>: the accuracy, evaluated by the Kappa coefficient [40], was larger than 0.8.

## 4. Results and Discussion

By using the spatial information of the land use zoning plan of Bangkok reported in Figure 2, the aim of the work is the analysis of the SUHI intensities within the different categories to assess their potential heating variability: such analysis is also useful to get indications on the urban development policy in terms of sustainability.

First, an overview of the SUHI pattern of the whole urban area of Bangkok is provided. Figure 4 shows the seven SUHI maps obtained from the satellite passages of Table 1; the last panel represents the mean SUHI of the seven maps.

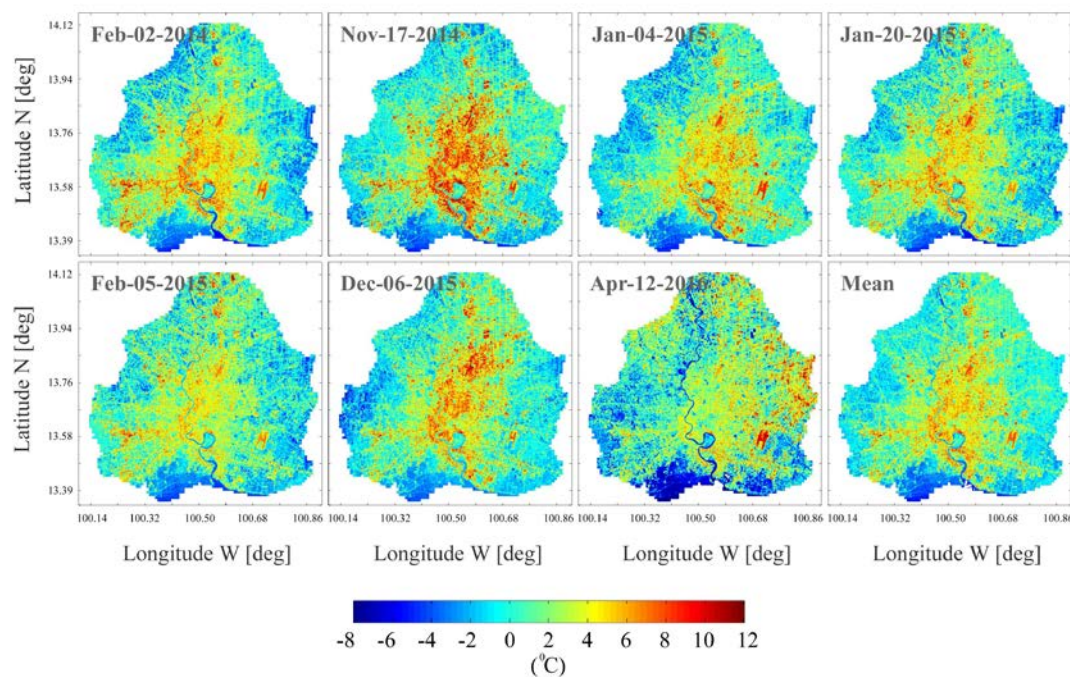


**Figure 4.** SUHI maps of Bangkok urban area obtained by the seven Landsat 8 clear-sky images. The last map represents the mean SUHI of the seven images.

The map of the 17 November 2014 shows the higher SUHI intensity, whilst the summer scene of April, the hottest month, exhibits a SUHI pattern in the urban area weaker than the other winter maps. In fact, despite a higher LST in April (the retrieved LST of the 12 April 2016 is around 45–50 °C in the built-up area, whilst in the same area the January and February LST is at least 10 degrees less), the reduced SUHI is ascribed to the summer warming of rural pixels and to the consequent increase of  $LST_{rural}$ , exerting a SUHI damping effect using Equation (1). Specifically, the rural zone in the east and north side of the map is made up of rice croplands. Paddy fields experience very different LST during the year, depending strongly on site-specific activities. Since rice harvesting finishes in December, rice areas are hot soils in summer during daytime, as well as other kinds of bare soils show hot surface temperatures. The RGB images of the seven Landsat scenes, not reported for the sake of simplicity, clearly reveal the different soil bareness or greenery of rural surrounding areas during the different months. Therefore, to have an average insight of the heating dynamics within the urban area, dampening the specific rural effects of each scene, the mean SUHI map of the seven Landsat images will be used in the comparison with the Bangkok land use zoning plan.

#### 4.1. SUHI within the Land Use Zoning Plan

The last comprehensive land use plan of Bangkok is superimposed on the mean SUHI map to single out the heating pattern of each class. In a potential action plan, this identification is the first step to provide a picture of the situation in the urban area. Then, the situation analysis allows to identify if specific categories in the land use plan require targeted future actions for the SUHI mitigation, or if the maintenance of the current urban model is in line with a sustainable development.

The land use plan superimposition on the mean SUHI map is shown in Figure 5. It is possible to notice that some hot built-up areas are outside the plan boundary.

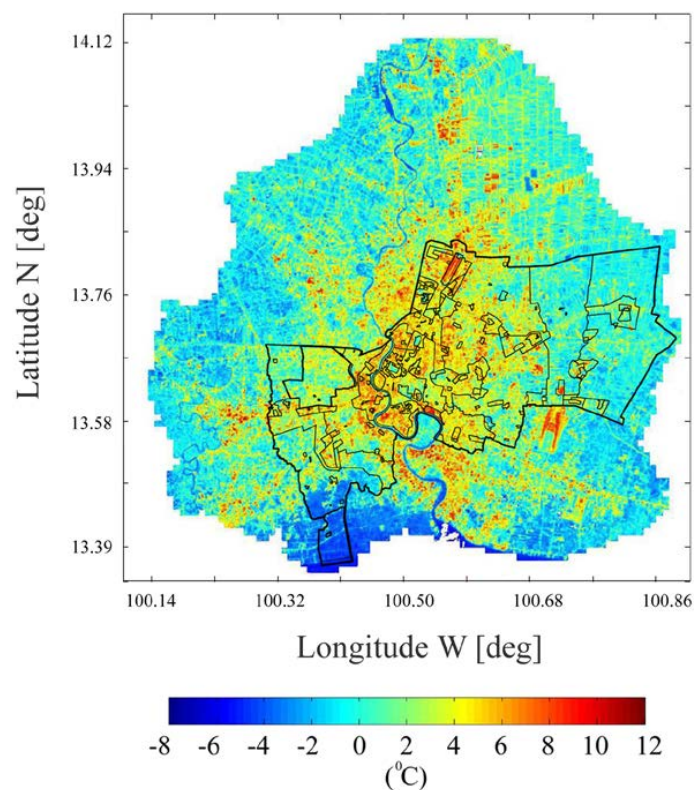


**Figure 5.** Mean SUHI map of Bangkok from Landsat 8 images (time interval 2014–2016) with the land use zoning plan of Figure 2 superimposed.

To better describe the SUHI pattern of each land use zone, a representation of the ten categories is reported in Figure 6. This figure depicts the layout of each category, its spatial extent and correspondent percentage within the whole plan, together with the superimposition on the mean SUHI map. Such representation allows to better identify the surface heating pattern of the different zones and to compute their SUHI statistics.

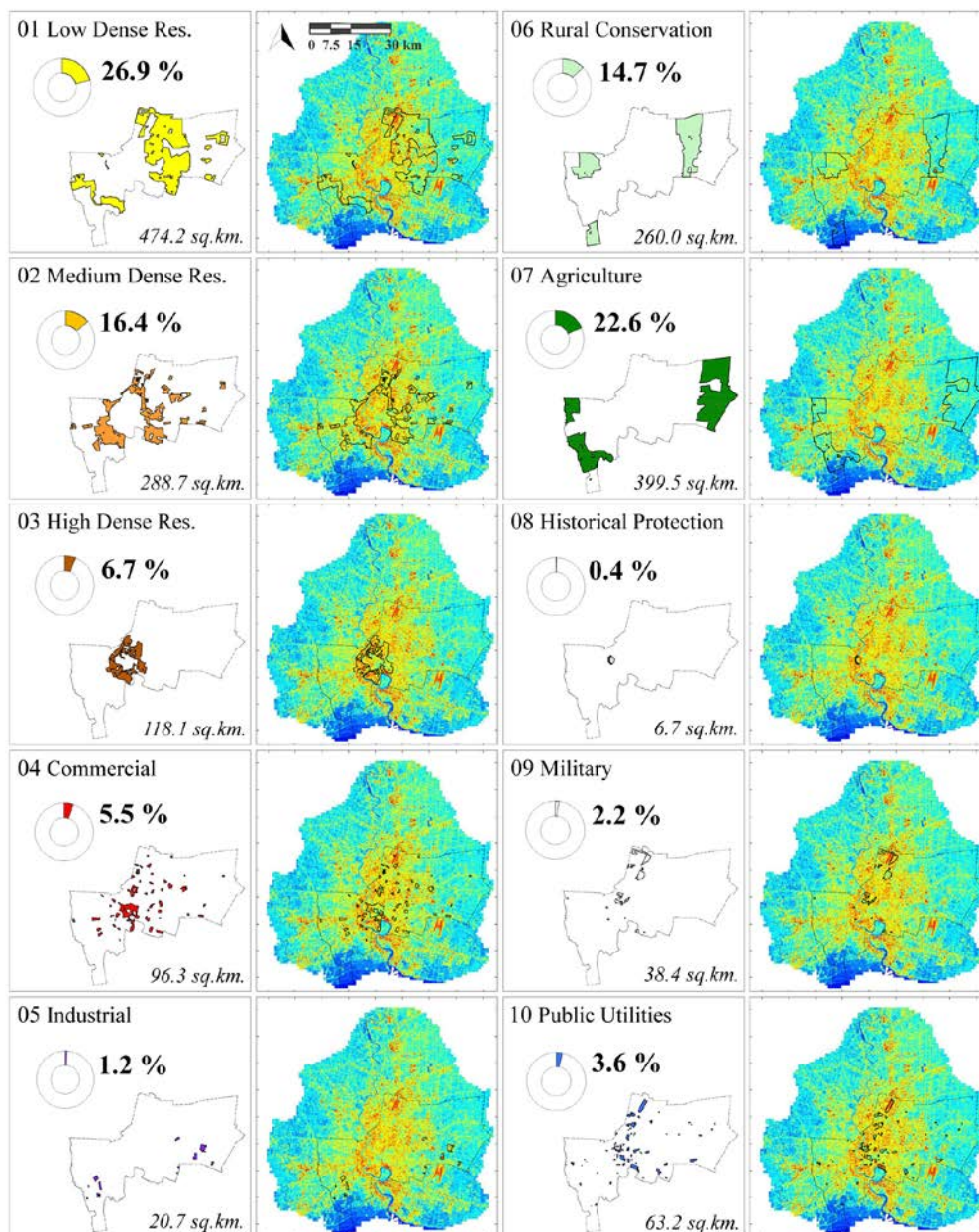


**Figure 6.** Representation of the ten categories of the Bangkok land use plan: layout, spatial extent and correspondent percentage within the whole plan, and superimposition on the mean SUHI map.

Considering the spatial extension of the different classes, the Landsat 8 pixel size of 100 m for the thermal channels, resampled at 30 m, is suitable for identifying the SUHI variability at the spatial scale of the land use plan categorization.

Figure 7 shows the main statistics of the SUHI intensity, temporal average of the seven maps, within the ten categories. The colored bars report, for each class, the mean SUHI intensity (black



horizontal line with value), whilst the bar length corresponds to  $\pm$ the standard deviation ( $\pm$ std). The maximum (red) and minimum (blue) SUHI values for each category are also reported.

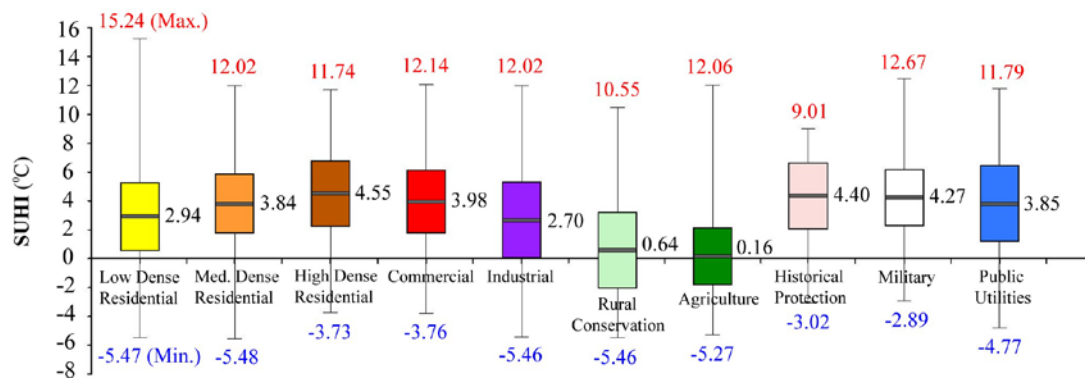


**Figure 7.** Main statistics of the SUHI intensity (temporal average of the seven SUHI maps) for the ten land use categories (the bar colors correspond to the legend of Figure 2). Each bar reports the mean SUHI intensity (black horizontal line with value) and the standard deviation ( $\pm$ std, length of the bar). The maximum (red) and minimum (blue) SUHI values for each category are also reported.

The negative minimum values for all the ten categories are due to greenery pixels: however, the vegetation extent and effects are clearly different within each class. Similarly, the maximum values over 10 °C suggest the presence of hot spot areas, even though their extensions can be very variable for each category.

As expected, the Rural Conservation and the Agricultural zones, among the wider ones, exhibit the lowest mean SUHI intensities, around 0 °C; the maximum values (10.5 °C and 12 °C) correspond both to dark roofs (i.e., low albedo surfaces) of isolated factories, giving rise to isolated warm pixels.

Concerning the three residential zones, it is interesting to note how the mean SUHI intensity increases from the Low-density to the High-density category, the latter having a lower mitigation effect from the LST ascribed to the vegetation pixels, as also suggested by the minimum SUHI value (−3.7 °C). From the layout of Figure 6, the warming effect of the High-density Residential zone is also ascribed to the placement in the city core, with less greenery amount and where the traffic congestion and the human activities are intense during daytime. Low-density Residential class is instead placed farther from the city center, benefiting of wider vegetation areas (the minimum SUHI value is −5.5 °C), as highlighted in Figure 6.

The same is true for the Commercial and Industrial classes: Commercial category, with higher mean SUHI (4 °C), is scattered in the whole plan area but with a quite evident concentration in the city center, whilst the Industrial zone, with a lower mean intensity (2.7 °C), is confined in the Bangkok outskirts. The benefit of some spotted green zones in the Industrial category is also confirmed by the lower minimum value (−5.5 °C). The Public Utilities/Government Institute class has a SUHI dynamic like the Commercial one, both having a quite similar spatial scattering.

The Historical Protection zone, the major tourist attraction, comprises the Thai Royal Palace surrounded by Old Historic temples: it is characterized by a high mean value of SUHI (4.4 °C) and a less cool minimum value (−3 °C). The Military zone has the same SUHI dynamics, with mean and minimum values of 4.3 °C and −2.9 °C, respectively. However, while the Historical Protection zone has the smallest spatial extension and very few vegetated pixels, the Military zone consists of base camps scattered in the Bangkok center and having larger green surfaces and tree canopy.

Overall, the analysis points out that the minimum SUHI of vegetated pixels is less cool when the category is placed in the city core (High-density Residential, Commercial, Historical and Military classes): such categories also exhibit the highest mean SUHI intensities (around or over 4 °C). The maximum SUHI intensity is, instead, quite independent from the category, since it can be ascribed

to isolate pixels that not necessarily follows the dynamic of the mean heating pattern, as seen previously for the Rural Conservation and the Agricultural zones.

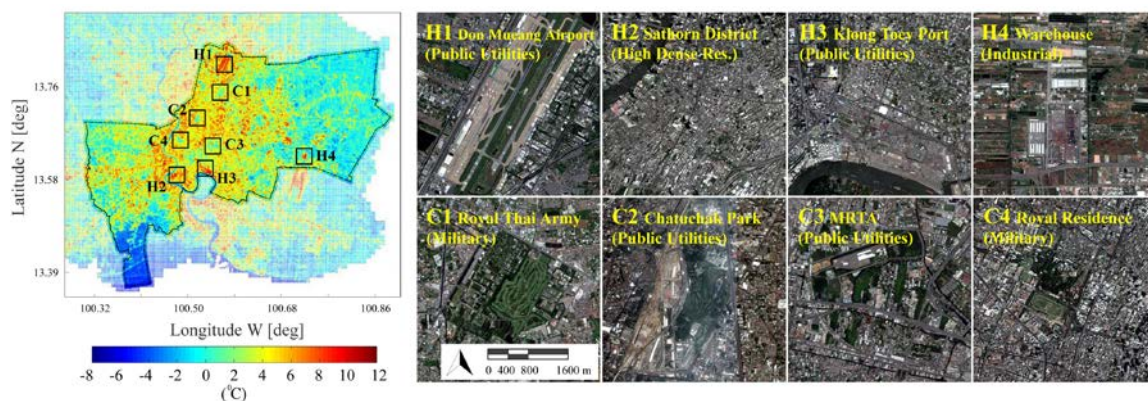
Since the above analysis has been performed over the last land use plan, it does not only describe the current situation, but also suggests that, for the categories mainly placed in the city center, the future urban development with further built-up areas will significantly hinder the SUHI mitigation, since the current surface cooling effects are weaker with respect to the other categories.

Although the information provided by the statistics of Figure 7 clearly describes the SUHI dynamics of each land use class, the pattern variability suggests that a more complete analysis requires the identification of evident mitigated or intense SUHI areas within some categories. Such analysis is reported in the next sub-section.

#### 4.2. Surface Urban Cool Island and Hot-Spotted Surfaces

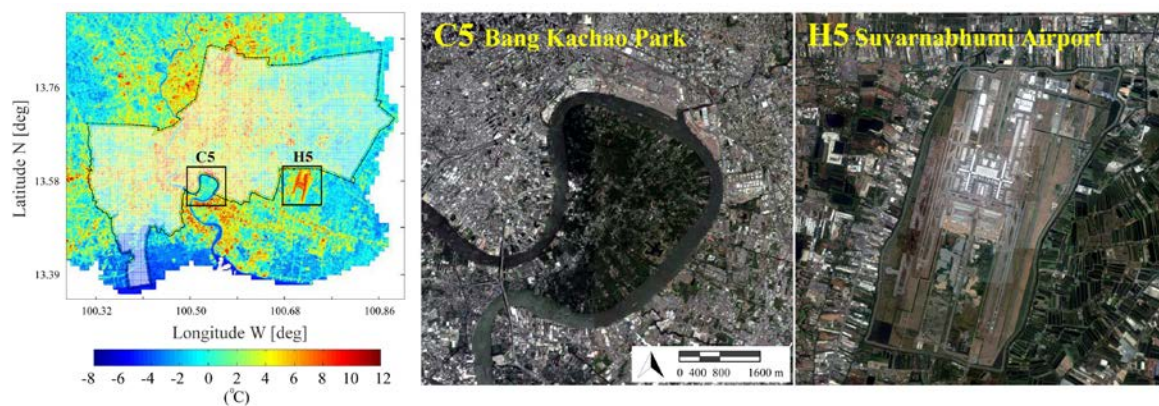
It is well known that urban green sites can be cooler than many built-up surfaces, producing the Surface Urban Cool Island (SUCI) phenomenon [9,41]. The assessment of the effect of city parks and urban greenery on the surface temperature is a good practice to understand if the developed city plan is in the direction of the UHI mitigation. Likewise, the identification of urban zones with very hot surfaces, henceforth named Hot-Spotted Surfaces (HSS), can help the designated municipal departments to single out priority zones for interventions and cooling actions.

Figure 8 shows some sites acting as SUCI (C1–C4, around 0 °C) and HSS (H1–H4, around 10 °C) within the land use plan, belonging to different categories. The RGB panels highlight the vegetation presence in the selected SUCI.



**Figure 8.** Examples of surface urban cool island (SUCI) (C1–C4) and hot-spotted surfaces (HSS) (H1–H4) within the land use zoning plan. In brackets the land use category of each site is reported. MRTA = Mass Rapid Transit Authority (of Thailand).

Two interesting wide sites outside the zoning plan exhibit a clear SUCI and HSS, as shown in Figure 9, clearly distinguishable regardless of the season in all the seven Landsat 8 images of Figure 4: The Bang Kachao Park and the Bangkok-Suvarnabhumi airport. The Bang Kachao Park is a 20 km<sup>2</sup> green area in an oxbow of the southern part of the Chao Phraya river, known as Bangkok’s green lung, exhibiting a mean SUHI intensity around 0 °C. Conversely, the HSS of Suvarnabhumi airport highlight a mean SUHI around 10 °C.



**Figure 9.** SUCI (C5, Bang Kachao Park) and HSS (H5, Suvarnabhumi airport) outside the land use plan boundary.

## 5. Conclusions

For many cities, the SUHI effect is an issue faced for several years. Actions to mitigate this problem should be integrated into the land use planning of the municipality. For instance, the maintenance and creation of cool areas within the city improve the quality of life and foster the sustainable development, helping to increase awareness of the SUHI issues in the population.

Since an action plan is based on the situation analysis, the identification of the SUHI intensity within the several urban categories (e.g., low/high density residential zone, commercial or industrial zone, etc.) is the first step. In this context, the SUHI maps derived from remote sensing sensors provide a scientific support for the municipal land use plan policy.

By means of Landsat imagery, this work shows how the SUHI maps can provide both an overview of the heating pattern across the whole city and a targeted analysis of delimited areas to identify detailed SUHI effects for focused future actions. The Landsat 8 TIRS channels, with a native pixel size of 100 m, has proved suitable for analyzing the surface thermal variability at the typical spatial scale of the urban land use classification.

**Author Contributions:** C.K. and S.B. conceived and designed the experiments; C.K. performed the experiments; C.K. and S.B. analyzed the data; S.B. wrote the paper.

**Conflicts of Interest:** The authors declare no conflict of interest.

## References

1. Fallmann, J.; Forkel, R.; Emeis, S. Secondary Effects of Urban Heat Island Mitigation Measures on Air Quality. *Atmos. Environ.* **2016**, *125*, 199–211. [[CrossRef](#)]
2. Chen, W.; Zhang, Y.; Pengwang, C.; Gao, W. Evaluation of Urbanization Dynamics and Its Impacts on Surface Heat Islands: A Case Study of Beijing, China. *Remote Sens.* **2017**, *9*, 453. [[CrossRef](#)]
3. Bhargava, A.; Lakmini, S.; Bhargava, S. Urban Heat Island Effect: It's Relevance in Urban Planning. *J. Biodivers. Endanger. Species.* **2017**, *5*, 5–187.
4. Liao, W.; Liu, X.; Wang, D.; Sheng, Y. The Impact of Energy Consumption on the Surface Urban Heat Island in China's 32 Major Cities. *Remote Sens.* **2017**, *9*, 250. [[CrossRef](#)]
5. Taha, H. Urban Climates and Heat Islands: Albedo, Evapotranspiration, and Anthropogenic Heat. *Energy Build.* **1997**, *25*, 99–103. [[CrossRef](#)]
6. Imhoff, M.L.; Zhang, P.; Wolfe, R.E.; Bounoua, L. Remote Sensing of the Urban Heat Island Effect across Biomes in the Continental USA. *Remote Sens. Environ.* **2010**, *114*, 504–513. [[CrossRef](#)]
7. Memon, R.A.; Leung, D.Y.C.; Chunho, L. A Review on the Generation, Determination and Mitigation of Urban Heat Island. *J. Environ. Sci.* **2008**, *20*, 120–128.
8. Voogt, J.A.; Oke, T.R. Thermal Remote Sensing of Urban Climates. *Remote Sens. Environ.* **2003**, *86*, 370–384. [[CrossRef](#)]

9. Rasul, A.; Balzter, H.; Smith, C.; Remedios, J.; Adamu, B.; Sobrino, J.A.; Srivani, M.; Weng, Q. A Review on Remote Sensing of Urban Heat and Cool Islands. *Land* **2017**, *6*, 38. [CrossRef]
10. Sobrino, J.; Oltra-Carrío, R.; Jimenez-Munoz, J.C.; Franch, B.; Hidalgo, V.; Mattar, C.; Julien, Y.; Cuenca, J.; Albentosa, M.R.R.; Gomez, J.A.; et al. Evaluation of the surface urban heat island effect in the city of Madrid by thermal remote sensing. *Int. J. Remote Sens.* **2013**, *34*, 3177–9192. [CrossRef]
11. Pichierri, M.; Bonafoni, S.; Biondi, R. Satellite Air Temperature Estimation for Monitoring the Canopy Layer Heat Island of Milan. *Remote Sens. Environ.* **2012**, *127*, 130–138. [CrossRef]
12. Anniballe, R.; Bonafoni, S.; Pichierri, M. Spatial and Temporal Trends of the Surface and Air Heat Island over Milan Using MODIS Data. *Remote Sens. Environ.* **2014**, *150*, 163–171. [CrossRef]
13. Azevedo, J.A.; Chapman, L.; Muller, C.L. Quantifying the Daytime and Night-Time Urban Heat Island in Birmingham, UK: A Comparison of Satellite Derived Land Surface Temperature and High Resolution Air Temperature Observations. *Remote Sens.* **2016**, *8*, 153. [CrossRef]
14. Li, Z.-L.; Tang, B.-H.; Wu, H.; Ren, H.; Yan, G.; Wan, Z.; Trigo, I.F.; Sobrino, J.A. Satellite-Derived Land Surface Temperature: Current Status and Perspectives. *Remote Sens. Environ.* **2013**, *131*, 14–37. [CrossRef]
15. Lin, T.; Sun, C.; Li, X.; Zhao, Q.; Zhang, G.; Ge, R.; Ye, H.; Huang, N.; Yin, K. Spatial Pattern of Urban Functional Landscapes along an Urban–rural Gradient: A Case Study in Xiamen City, China. *Int. J. Appl. Earth. Obs. Geoinf.* **2016**, *46*, 22–30. [CrossRef]
16. Deilami, K.; Kamruzzaman, M.; Hayes, J.F. Correlation or Causality between Land Cover Patterns and the Urban Heat Island Effect? Evidence from Brisbane, Australia. *Remote Sens.* **2016**, *8*, 716. [CrossRef]
17. Zhang, L.; Weng, Q.; Shao, Z. An Evaluation of Monthly Impervious Surface Dynamics by Fusing Landsat and MODIS Time Series in the Pearl River Delta, China, from 2000 to 2015. *Remote Sens. Environ.* **2017**, *201*, 99–114. [CrossRef]
18. Cao, X.; Onishi, A.; Chen, J.; Imura, H. Quantifying the Cool Island Intensity of Urban Parks Using ASTER and IKONOS Data. *Landsc. Urban Plan.* **2010**, *96*, 224–231. [CrossRef]
19. Susca, T.; Gaffin, S.R.; Dell’Osso, G.R. Positive Effects of Vegetation: Urban Heat Island and Green Roofs. *Environ. Pollut.* **2011**, *159*, 2119–2126. [CrossRef] [PubMed]
20. Gago, E.J.; Roldan, J.; Pacheco-Torres, R.; Ordóñez, J. The City and Urban Heat Islands: A Review of Strategies to Mitigate Adverse Effects. *Renew. Sust. Energ. Rev.* **2013**, *25*, 749–758. [CrossRef]
21. Zhou, B.; Rybski, D.; Kropp, J.P. The Role of City Size and Urban Form in the Surface Urban Heat Island. *Sci. Rep.* **2017**, *7*, 4791. [CrossRef] [PubMed]
22. MacLachlan, A.; Biggs, E.; Roberts, G.; Boruff, B. Urbanisation-Induced Land Cover Temperature Dynamics for Sustainable Future Urban Heat Island Mitigation. *Urban Sci.* **2017**, *1*, 38. [CrossRef]
23. Jongtanom, Y.; Kositanont, C.; Baulert, S. Temporal Variations of Urban Heat Island Intensity in Three Major Cities, Thailand. *Mod. Appl. Sci.* **2011**, *5*, 105. [CrossRef]
24. Arifwidodo, S.D.; Tanaka, T. The Characteristics of Urban Heat Island in Bangkok, Thailand. *Procedia Soc. Behav. Sci.* **2015**, *195*, 423–428. [CrossRef]
25. Arifwidodo, S.; Chandrasiri, O. Urban Heat Island and Household Energy Consumption in Bangkok, Thailand. *Energy Procedia.* **2015**, *79*, 189–194. [CrossRef]
26. Tran, H.; Uchiyama, D.; Ochi, S.; Yasuoka, Y. Assessment with Satellite Data of the Urban Heat Island Effects in Asian Mega Cities. *Int. J. Appl. Earth. Obs. Geoinf.* **2006**, *8*, 34–48. [CrossRef]
27. Thaiutsa, B.; Puangchit, L.; Kjelgren, R.; Arunpraparut, W. Urban Green Space, Street Tree and Heritage Large Tree Assessment in Bangkok, Thailand. *Urban For. Urban Green.* **2008**, *7*, 219–229. [CrossRef]
28. Thai Meteorological Department. Available online: <https://www.tmd.go.th/en/climate.php> (accessed on 20 December 2017).
29. Department of Public Works and Town & Country Planning. Available online: <https://dpt.go.th/en/> (accessed on 3 January 2018).
30. US Geological Survey USGS. Available online: <http://earthexplorer.usgs.gov> (accessed on 12 December 2017).
31. Yu, X.; Guo, X.; Wu, Z. Land Surface Temperature Retrieval from Landsat 8 TIRS—Comparison between Radiative Transfer Equation-Based Method, Split Window Algorithm and Single Channel Method. *Remote Sens.* **2014**, *6*, 9829–9852. [CrossRef]
32. Jimenez-Munoz, J.C.; Cristobal, J.; Sobrino, J.A.; Soria, G.; Ninyerola, M.; Pons, X. Revision of the Single-Channel Algorithm for Land Surface Temperature Retrieval From Landsat Thermal-Infrared Data. *IEEE Trans. Geosci. Remote Sens.* **2009**, *47*, 339–349. [CrossRef]

33. Atmospheric Correction Parameter Calculator. Available online: <http://atmcorr.gsfc.nasa.gov> (accessed on 22 December 2017).
34. Barsi, J.A.; Barker, J.L.; Schott, J.R. An Atmospheric Correction Parameter Calculator for a Single Thermal Band Earth-Sensing Instrument. In Proceedings of the IEEE International Geoscience and Remote Sensing Symposium (IGARSS) (IEEE Cat. No.03CH37477), Toulouse, France, 21–25 July 2003; Volume 5, pp. 3014–3016.
35. Sobrino, J.A.; Jiménez-Muñoz, J.C.; Paolini, L. Land Surface Temperature Retrieval from LANDSAT TM 5. *Remote Sens. Environ.* **2004**, *90*, 434–440. [[CrossRef](#)]
36. Bonafoni, S. Downscaling of Landsat and MODIS Land Surface Temperature Over the Heterogeneous Urban Area of Milan. *IEEE J. Sel. Top. Appl. Earth Obs. Remote Sens.* **2016**, *9*, 2019–2027. [[CrossRef](#)]
37. Oltra-Carrio, R.; Sobrino, J.A.; Franch, B.; Nerry, F. Land surface emissivity retrieval from airborne sensor over urban areas. *Remote Sens. Environ.* **2012**, *123*, 298–305. [[CrossRef](#)]
38. Bolstad, P.V.; Lillesand, T.M. Rapid Maximum Likelihood Classification. *Photogramm. Eng. Remote Sens.* **1991**, *57*, 67–74.
39. Phiri, D.; Morgenroth, J. Developments in Landsat Land Cover Classification Methods: A Review. *Remote Sens* **2017**, *9*, 967. [[CrossRef](#)]
40. Jensen, J.R. *Introductory Digital Image Processing: A Remote Sensing Perspective*, 4 ed.; Pearson: Glenview, IL, USA, 2015.
41. Yang, C.; He, X.; Yu, L.; Yang, J.; Yan, F.; Bu, K.; Chang, L.; Zhang, S. The Cooling Effect of Urban Parks and Its Monthly Variations in a Snow Climate City. *Remote Sens.* **2017**, *9*, 1066. [[CrossRef](#)]



© 2018 by the authors. Licensee MDPI, Basel, Switzerland. This article is an open access article distributed under the terms and conditions of the Creative Commons Attribution (CC BY) license (<http://creativecommons.org/licenses/by/4.0/>).